Chapter VI : Influence of Strain-induced Phase Transformations on the Mechanical Properties of Fe-Ni-Cr and Fe-Mn-Si-Al Steel Grades

VI.1 Introduction

Stainless and other highly-alloyed steel grades are good candidates for applications where corrosion resistance and excellent mechanical

properties have to be combined. However, it has been shown in Chapter V that mechanically-induced phase transformations considerably modify the microstructure during straining. Parameters such as chemical composition, temperature, grain size and stress state are known to present a large influence on the phase transformations. The interactions between these factors, the phase transformations and the mechanical properties are of primary importance to determine the forming parameters for an industrial use.

As it was presented in Chapter I, the two main parameters that dictate the phase transformations are the relative stability of the phases and the stacking fault energy (SFE) of the austenite. Indeed, the stability defines which phase will form and the SFE determines the mechanisms of phase transformations. Chapter V investigated the mechanisms of the phase transformations taking place during uniaxial tension, cold rolling and rotary swaging. The objectives of this chapter are twofold :

1) to study the phase transformations at a macroscopic scale in several steel grades ;
2) to investigate the influence of the different phases and phase transformations on the mechanical properties.

Specifically, the influence of various parameters such as chemical composition, strain rate and temperature, austenitic grain size and stress state will be examined.

The chemical composition has a major influence on the phase transformations. Firstly, it modifies the stability of the austenite.

Indeed, elements like Ni, C or Mn stabilise the austenite while others like Cr, Si or Al favour the formation of ferrite [Laco90]. In Fe-Mn alloys, a Mn content larger than 16wt.% brings about the formation at low temperature of the HCP phase instead of the BCC phase, as shown by Figure VI.1 [Verc04]. Moreover, most alloying elements tend to stabilise the austenite against martensitic transformation [Laco90], due to the perturbation in the atomic movements at low temperatures.

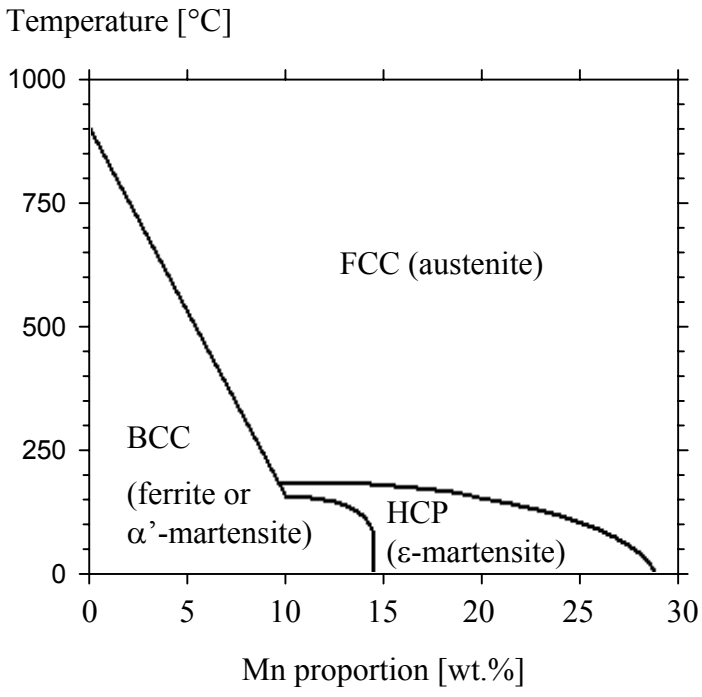

Figure VI.1 : Metastable Fe-Mn binary phase diagram. The transition lines represent the start temperature for the phase transformations (from [Verc04]).

Besides the phase stability, the chemical composition also influences the SFE of the austenite. In the high-manganese steel grades studied in this thesis, three alloying elements are present : Al, Si and Mn. Al increases the SFE [Char81, Oh95, Chen93] while Si decreases it [Furu89, Gras98, From03]. Increasing the manganese content first tends to decrease the SFE down to a minimum before increasing it again. The minimum SFE (about 11mJ/m²) is reached for a Mn content of about 14 at.% (*i.e.* 13.8 wt.%) [Cotes04]. In austenitic stainless steels, it has been shown that Ni and C increase the SFE, while Cr and N decrease it [Laco90].

The temperature and the grain size also affects the SFE. Indeed, a higher temperature stabilises the austenite and increases the SFE [Tomo91, Dai03, Dai04]. Moreover, reducing the austenitic grain size also increases the stability of the austenite and the SFE [Jun98, Lee00, Talo04].

Finally, the influence of the stress state is directly related to the relationship between the applied stress, the orientation of the grains and the transformation strain. As presented in Chapter V, the variant selection process determines which variant can actually form under a given stress level and according to the crystallographic possibilities. Moreover, the stress triaxiality also influences the phase transformations [Good70, Lebe00].

VI.2 Materials and Experimental Procedure

Four different grades are studied in this Chapter : steels 301LN and 304, which are fully austenitic Ni-Cr stainless steels, and steels Mn15 and Mn20, which are Fe-Mn-Si-Al alloys. The chemical compositions of these grades are reminded in Table VI.1.

wt. %	C	Mn	Al	Si
301LN	0.027	1.3	< D. L.	0.43
304	0.02	1.85	< D. L.	0.56
Mn15	$1.6\ 10^{-3}$	15.99	3.08	2.80
Mn20	$1.7\ 10^{-3}$	19.66	3.11	2.88

wt. %	Cr	Ni	Mo	N
301LN	17.51	6.59	0.16	0.012
304	18.22	9.03	0.18	0.037
Mn15	< D. L.	< D. L.	< 0.005	$5.3\ 10^{-5}$
Mn20	< D. L.	< D. L.	< 0.005	$5.7\ 10^{-5}$

Table VI.1 : Chemical compositions of the different steel grades. (D.L. stands for Detection Limit)

Steels Mn15 and Mn20 were hot-rolled and then annealed for 1h at 900°C, 1000°C or 1100°C. Figure VI.2 reminds the phase proportions in steels Mn15 (Figure VI.2 (a)) and Mn20 (Figure VI.2 (b)) after the annealing treatment of 1 hour at these different temperatures, as presented in Chapter III. This Figure shows that the proportion of ferrite increases with the annealing temperature in steel Mn15 and remains almost unchanged in steel Mn20.

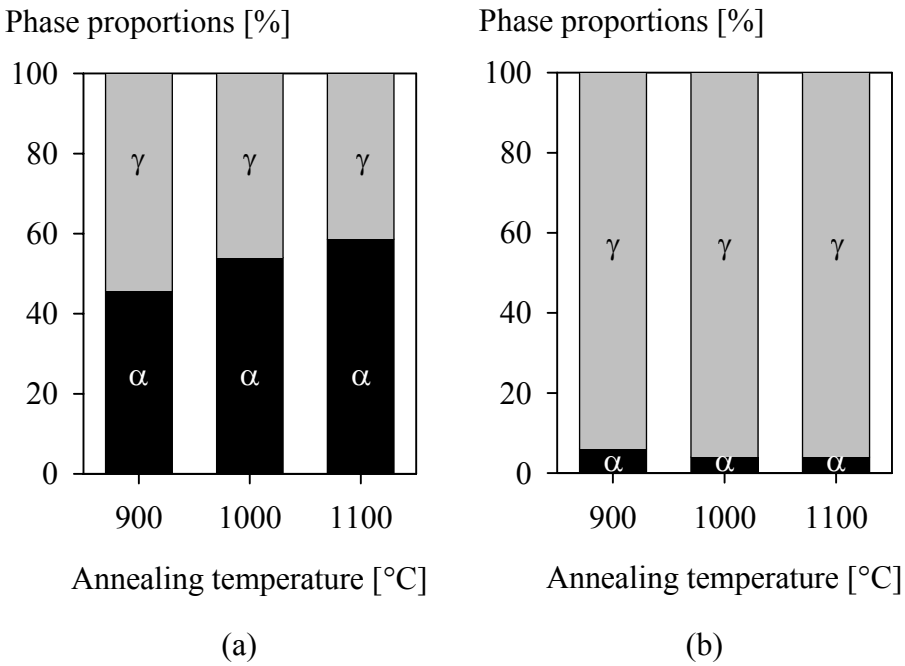

Figure VI.2 : Phase proportions in steels (a) Mn15 and (b) Mn20 annealed for1h at 900°C, 1000°C or 1100°C, respectively.

Figure VI.3 shows the austenite grain size in steels Mn15 and Mn20 after the annealing treatments (Chapter III). It can be seen that the austenite grain size is smaller in steel Mn15 than in steel Mn20.

Moreover, a higher annealing temperature generally induces a larger grain size, except for the sample Mn20 1100.

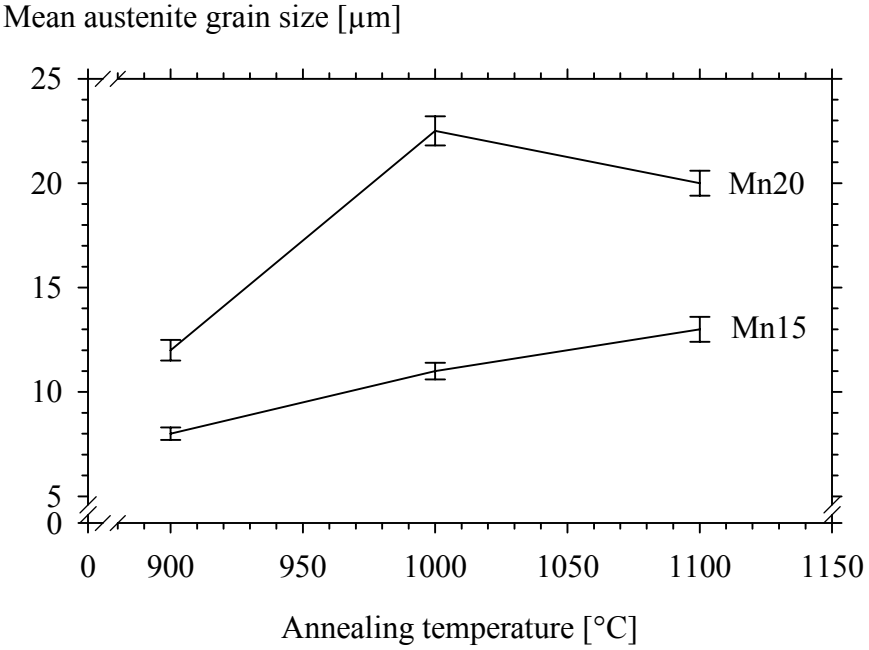

Figure VI.3 : Evolution of the mean austenite grain size with annealing temperature for steels Mn15 and Mn20 annealed for 1h at 900°C, 1000°C or 1100°C.

The mechanical properties and the evolution of the phase proportions were measured for uniaxial tension conditions. Moreover, the phase transformations occurring during cold-rolling and rotary swaging were monitored for steel 301LN. The phase proportions were measured by X-ray diffraction (XRD) in unloaded samples or by neutron diffraction during *in situ* tensile tests. Moreover, the lattice

parameters were obtained by fitting the neutron diffraction spectra. The mean lattice strain is defined for each phase as :

$$\varepsilon^{lat.} = \frac{d^{lat.} - d_0^{lat.}}{d_0^{lat.}} \quad \text{(VI.1)}$$

where $d_0^{lat.}$ represents the initial stress-free lattice parameter and $d^{lat.}$, the instantaneous lattice parameter during loading.

VI.3 Results

VI.3.1 Mechanical properties and strain-induced phase transformations during tensile straining

The tensile true stress *vs.* true strain curves of steels Mn15 and Mn20 annealed for 1h at different temperatures are shown in Figure VI.4. It can be seen that steel Mn15 presents a higher strength but a lower uniform elongation than steel Mn20. For both grades, a higher annealing temperature brings about a higher uniform elongation and lower values of yield strength. As far as the true stress at maximum load is concerned, no clear difference is observed between the different annealing temperatures, except for the sample Mn20 1100, which presents a lower maximum true stress. For both steel grades, a change of slope of the true stress *vs* true strain curves can be observed, even though it is less marked for the sample Mn20 1100.

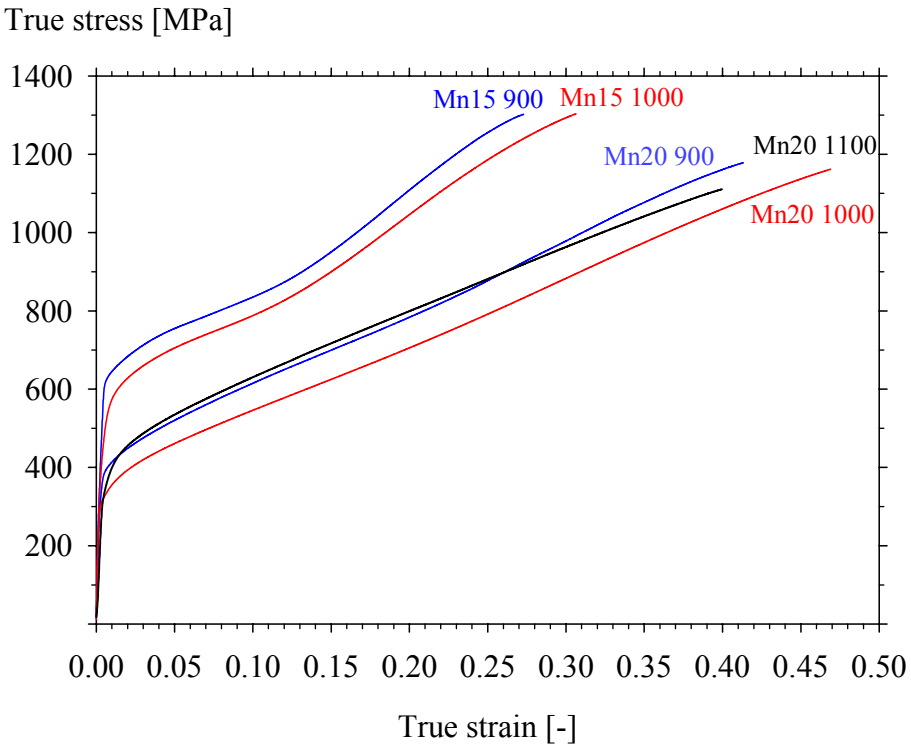

Figure VI.4 : True stress vs. true strain tensile curves of steels Mn15 and Mn20 annealed for 1 hour at 900°C, 1000°C or 1100°C.

Figure VI.5 presents the evolution of the maximum true uniform strain (ε_u) as a function of the different annealing temperatures of steels Mn15 and Mn20. For both steels, ε_u is larger for the samples annealed at 1000°C than for the samples annealed at 900°C. Furthermore, the sample Mn20 1100 presents the smallest ε_u among all Mn20 samples.

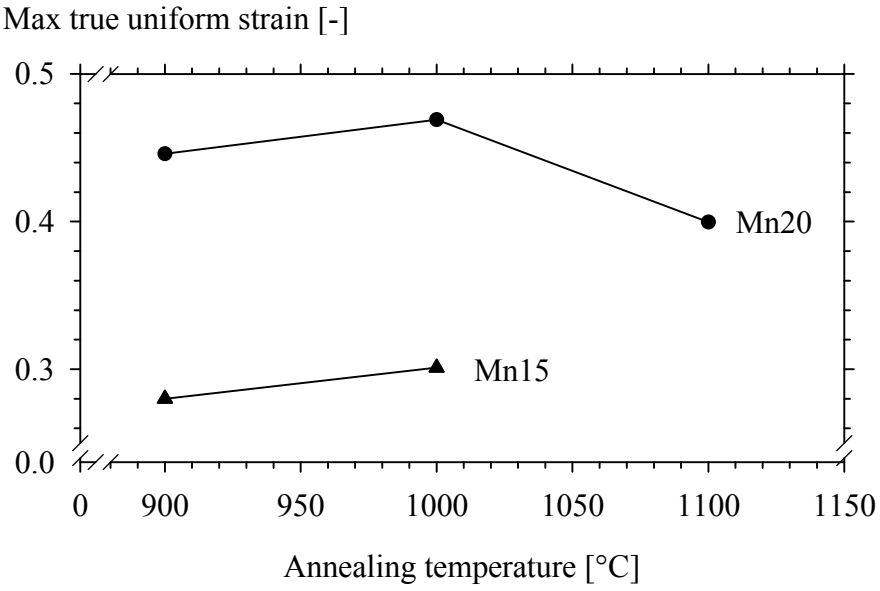

Figure VI.5 : Maximum true uniform strain for steels Mn15 and Mn20 annealed for 1h at 900°C, 1000°C or 1100°C.

Figure VI.6 shows the evolution of the work-hardening rate with true strain for steel Mn15 annealed for 1h at 900°C or 1000°C (Figure VI.6 (a)) and steel Mn20 annealed for 1h at 900°C, 1000°C or 1100°C (Figure VI.6 (b)), respectively. Theses figures clearly show that for both grades, $n_{incr.}$ first increases then decreases down to the point where the Considere criterion for necking is fulfilled ($n = \varepsilon$). Samples of steel Mn15 present a steep increase of the work-hardening rate around $\varepsilon = 0.1$ while $n_{incr.}$ starts to decrease for $\varepsilon \approx 0.2$. Sample Mn15 1000 presents a smoother decrease of $n_{incr.}$. In the case of samples of steel Mn20, the change of slope is very small and occurs around $\varepsilon \approx 0.2$. However, no clear change can be observed for the sample Mn20 1100. Sample Mn20 900 presents a steeper decrease of $n_{incr.}$ after the maximum.

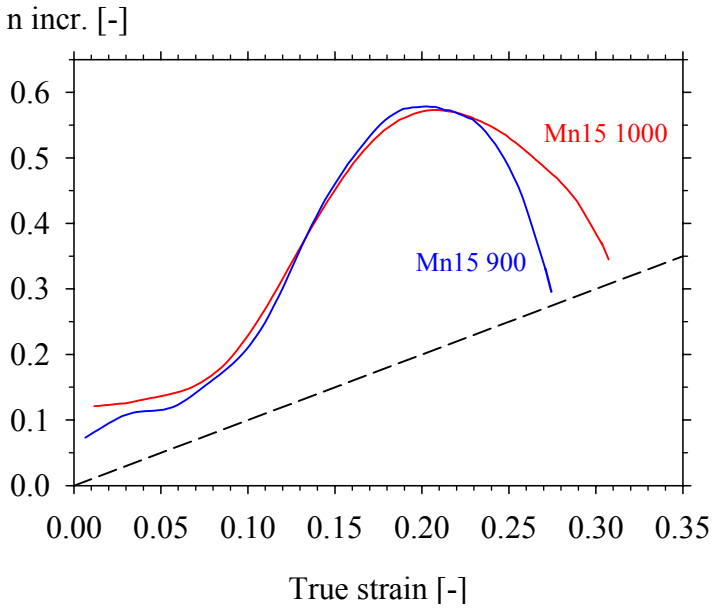

(a)

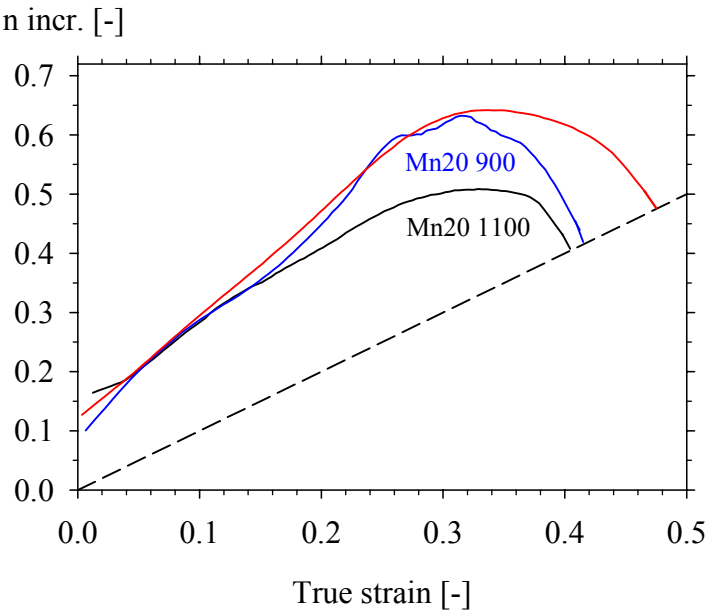

(b)

Figure VI.6 : Evolution of $n_{incr.}$ with true strain
(a) for steel Mn15 annealed for 1h at 900°C or 1000°C ;
(b) for steel Mn20 annealed for1h at 900°C, 1000°C or 1100°C.
(the dashed lines correspond to the Considere instability criterion).

Figure VI.7 presents the evolution of the mean lattice strain in austenite and ferrite during the first stages of tensile deformation of steel Mn15 1000. The evolution of the lattice strain is similar for both phases until $\varepsilon^{lat.} \approx 0.0015$, then a first inflexion point can be observed in the ferrite curve. When its mean lattice strain reaches about 0.005, a second inflexion points is visible in the ferrite curve, then the evolution starts to be erratic.

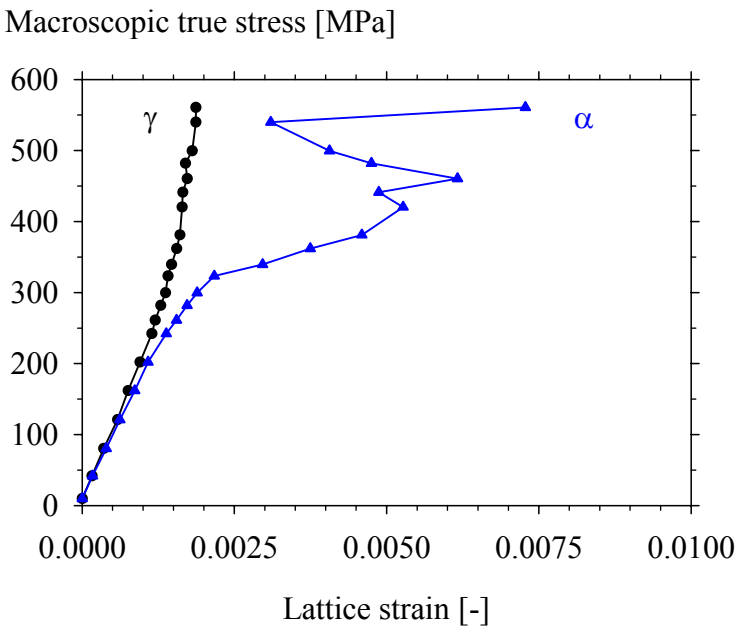

Figure VI.7 : Lattice strain vs. macroscopic true stress for austenite (γ) and ferrite (α) in sample Mn15 1000 during the first stages of tensile deformation.

The evolutions of the phase proportions during tensile straining have been measured as described in section II.2.1.3, by X-ray diffraction on unloaded specimens or *in situ* by neutron diffraction.

Figure VI.8 presents the evolution of phase proportions during tensile straining of steel Mn15 annealed for 1h at 900°C (Figure VI.8 (a)) or 1000°C (Figure VI.8 (b)). The measurements were performed by X-ray diffraction for steel Mn15 900 and by neutron diffraction for steel Mn15 1000. It must be noticed that the content of ferrite, which is not influenced by straining, is not represented on Figure VI.8. The proportion of austenite continuously decreases along straining so that it almost completely disappears at the onset of necking. On the other hand, α'-martensite forms all along straining. However, after a strain of ε = 0.05 – 0.07, its rate of formation increases. Finally, the proportion of ε-martensite first increases, reaches a maximum (around ε = 0.1 – 0.12) then decreases slowly. It can be observed that more ε-martensite forms in steel Mn15 1000 while more α'-martensite forms in steel Mn15 900.

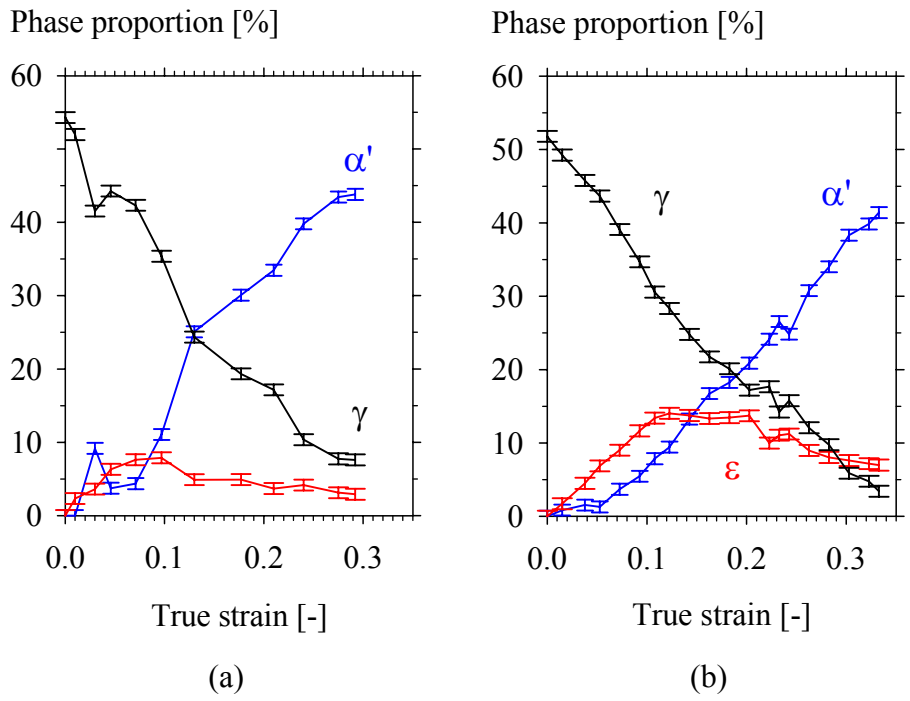

Figure VI.8 : Evolution of phase proportions during tensile straining of steels (a) Mn15 900 and (b) Mn15 1000.

Figure VI.9 presents the evolution of phase proportions during tensile straining of steel Mn20 annealed for 1h at 900°C (Figure VI.9 (a)) or 1000°C (Figure VI.9 (b)). These proportions were measured by X-ray diffraction in steel Mn20 900 and neutron diffraction in steel Mn20 1000. It can be observed that the austenite transforms with a transformation rate that decreases with straining. In steel Mn20 1000, the austenite proportion stabilises around $\varepsilon = 0.32$ and 32% of austenite remains untransformed at necking. On the other hand, α'-martensite forms continuously all along straining while the proportion of ε-martensite first increases, reaches a maximum (around

ε = 0.2 – 0.25) then slowly decreases. Finally, more ε-martensite forms in the sample Mn20 1000 while the proportion of α'-martensite is higher in sample Mn20 900.

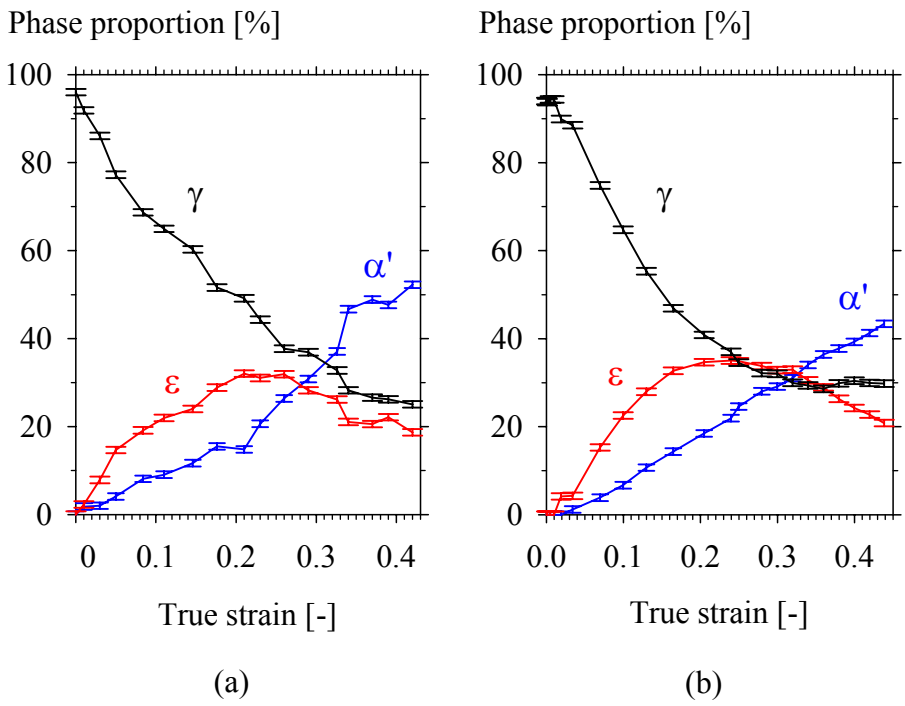

Figure VI.9 : Evolution of phase proportions during tensile straining of steels (a) Mn20 900 and (b) Mn20 1000.

Figure VI.10 presents the tensile true stress *vs.* true strain curves of steels 301LN and 304. Steel 301LN presents a yield strength which is slightly larger than the yield strength of steel 304. However, a very different work-hardening behaviour of both steel grades leads to very different mechanical properties : steel 301LN exhibits a larger true stress at maximum load but a lower true strain than steel 304.

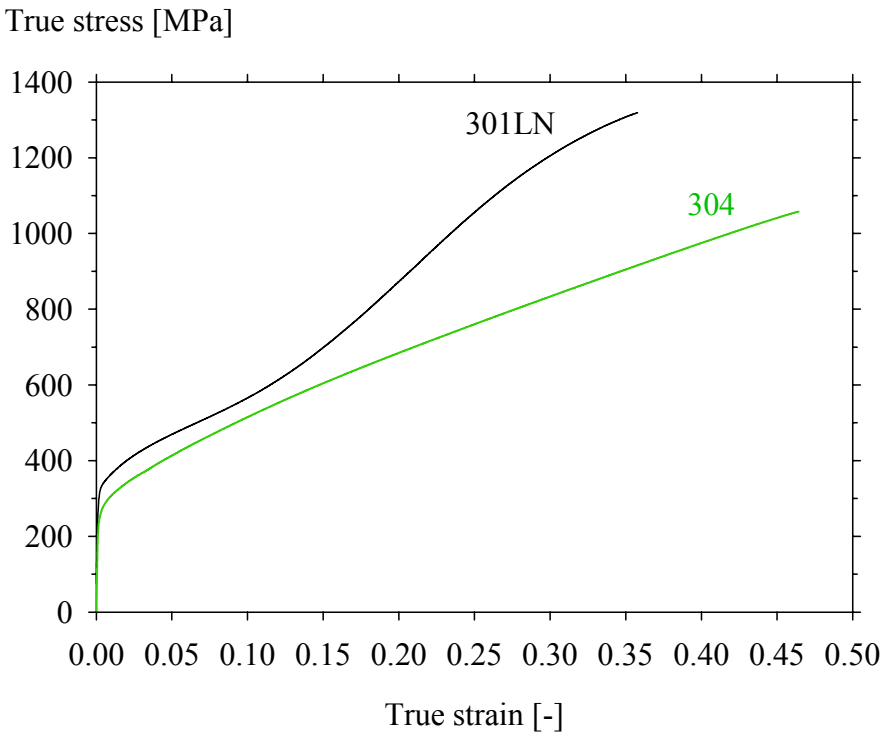

Figure VI.10 : Tensile true strain vs. true stress curves of steels 304 and 301LN.

Figure VI.11 shows the evolution of the work-hardening rate during tension of steels 301LN and 304. The evolution is similar for both grades up to $\varepsilon = 0.08$. Then, the work-hardening rate of steel 301LN increases abruptly, reaches a maximum at $\varepsilon = 0.22$ then decreases. The evolution of the work-hardening rate of steel 304 remains more monotonous : $n_{incr.}$ increases continuously almost up to necking.

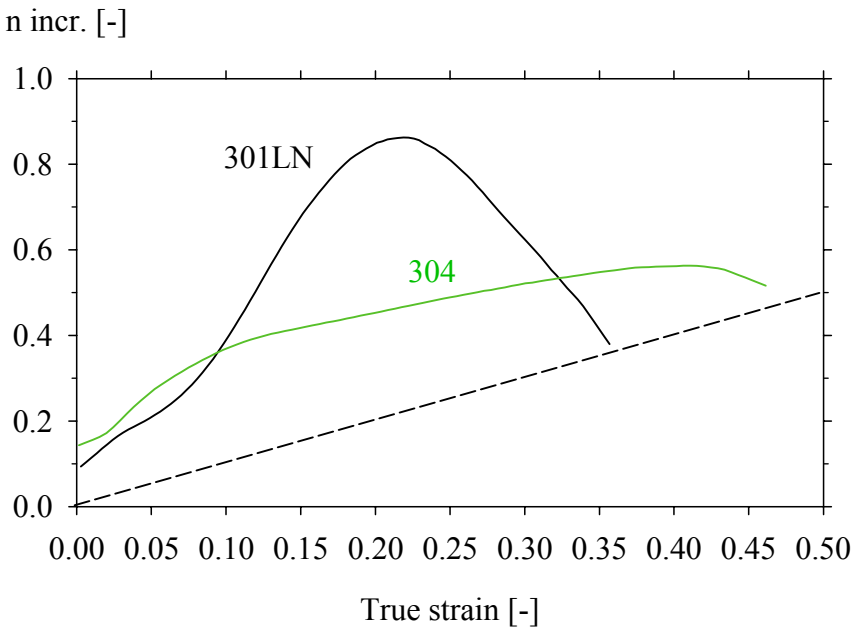

Figure VI.11 : Evolution of $n_{incr.}$ during tensile straining of steels 301LN and 304. (the dashed line corresponds to the Considere instability criterion).

Typical tensile true stress – true strain curves of steel 301LN presenting three grain sizes of 1.2µm, 11µm or 41.8µm, respectively, are presented in Figure VI.12. These curves show that the true stress at maximum load (σ_u) decreases while the true uniform strain (ε_u) increases when the grain size increases. Moreover, all samples present a change of slope, which indicates that the work-hardening rate varies during straining.

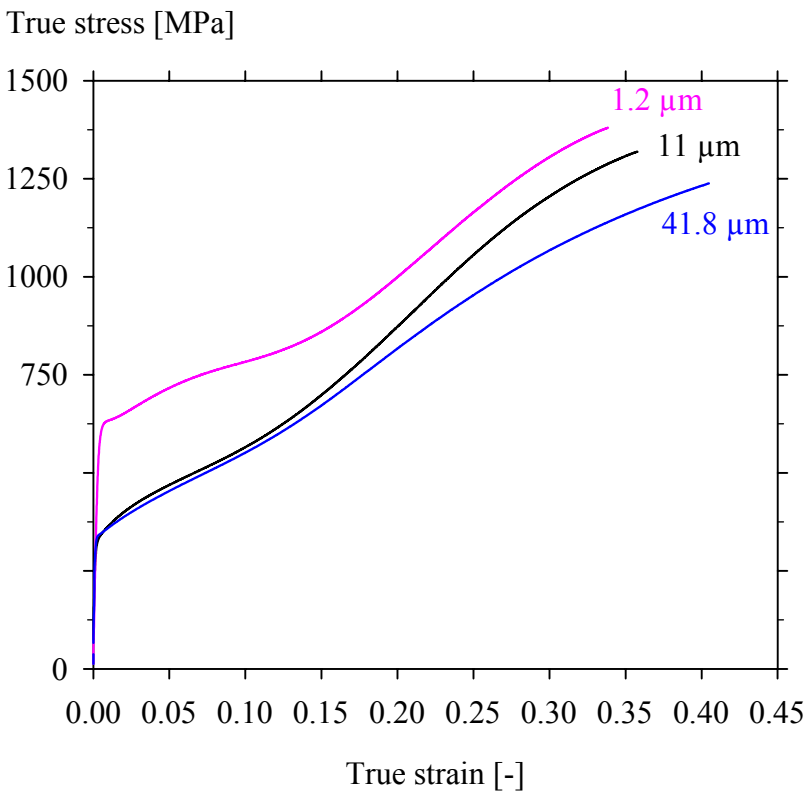

Figure VI.12 : Tensile true stress vs. true strain curves of steel 301 LN with 3 different grain sizes (1.2µm, 11µm or 41.8 µm).

Figure VI.13 shows the evolution of the work-hardening rate during tensile straining of steel 301LN presenting three different grain sizes (1.2µm, 11µm or 41.8µm). The evolution of the work-hardening rate with the deformation shows an inflexion point in the first part of the curve. The rise of the work-hardening rate occurs later as the grain size is reduced. In the sample with the smallest grain size, this brings about a stage in the evolution of the work-hardening rate (up to about $\varepsilon = 0.1$) before $n_{incr.}$ rises. The maximum of the work-hardening rate is reached sooner when the grain size is larger, but the descending slope

is much softer for the sample with large grains, leading to a higher true uniform strain.

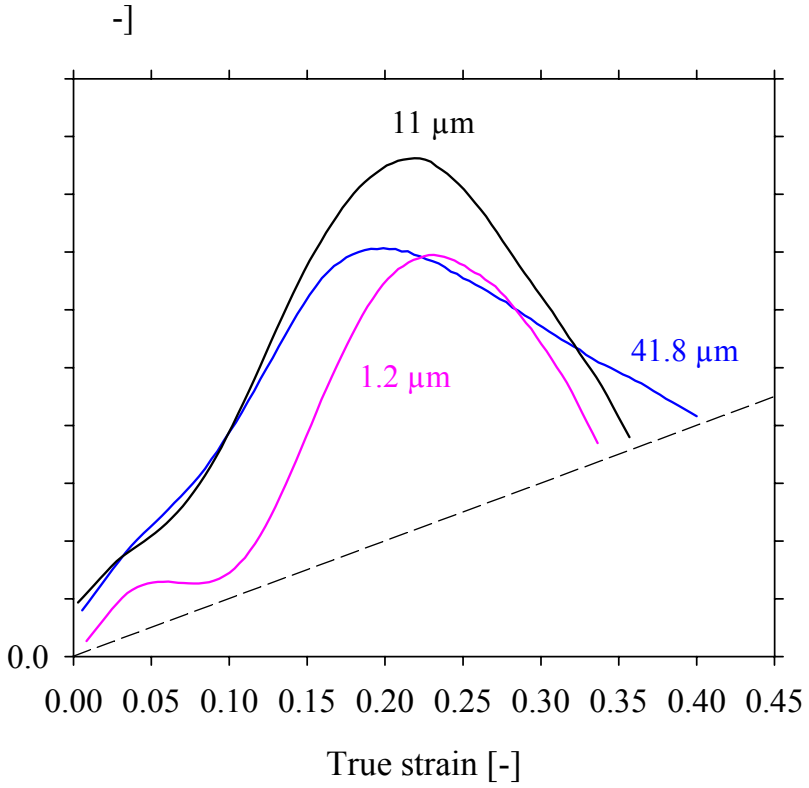

Figure VI.13 : Evolution of $n_{incr.}$ during tensile test of steel 301LN with three different grain sizes (1.2 µm, 11 µm or 41.8 µm). (the dashed line corresponds to the Considere instability criterion).

The evolutions of the phase proportions during tensile straining of steel 301LN with two different grain sizes (1.2µm or 11µm) are presented in Figure VI.14. The transformation in both samples is globally similar. However, the transformation rate is smaller for the specimen with the smaller grain size. Moreover, the transformation

does not seem monotonous in the small grained sample. Indeed, the transformation seems very high in the early stages of straining, then slows down at $\varepsilon = 0.03$, then increases abruptly around $\varepsilon = 0.13$.

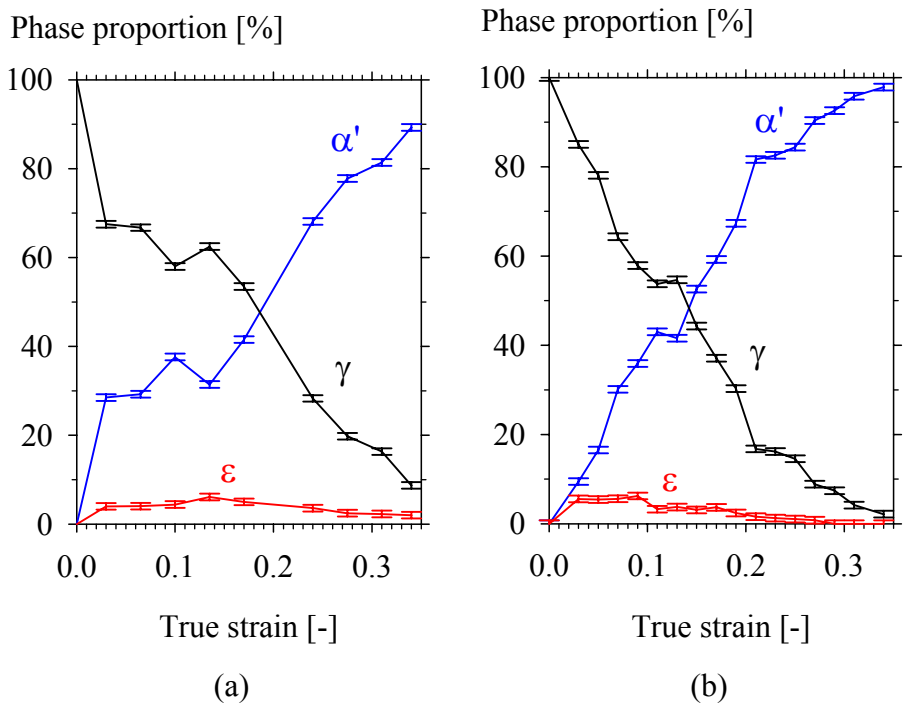

Figure VI.14 : Evolution of the phase proportions during tensile straining of steel 301LN with 2 different grain sizes : (a) 1.2µm or (b) 11µm.

Figure VI.15 (a) shows tensile true stress – true strain curves of steel 301LN tested at two different strain rates, 10^{-4} s^{-1} or 3 . 10^{-3} s^{-1}, respectively. Figure VI.15 (b) presents the evolution of the sample temperature during straining. A higher strain rate decreases the stress at maximum load and true uniform strain (σ_u and ε_u). Moreover, a change of slope can be observed for both strain rates, but it is less

marked for the sample tested with the highest strain rate. It must also be noted that the higher strain rate brings about a progressive rise of the temperature of the sample.

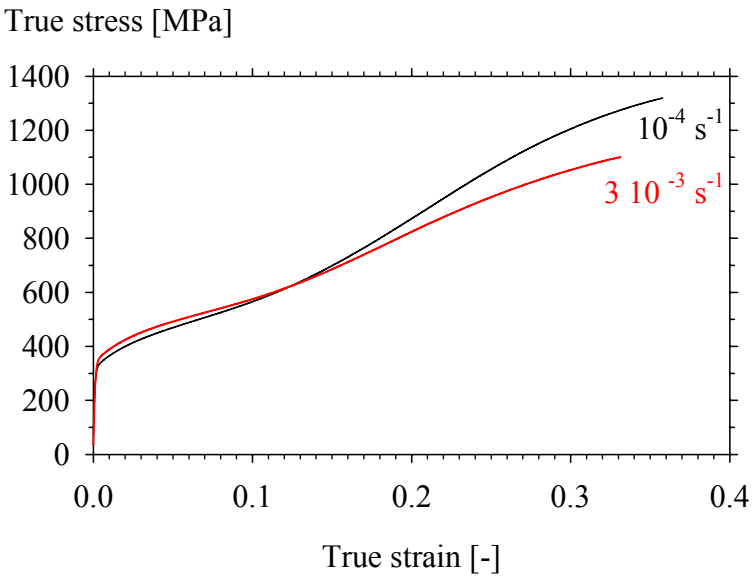

(a)

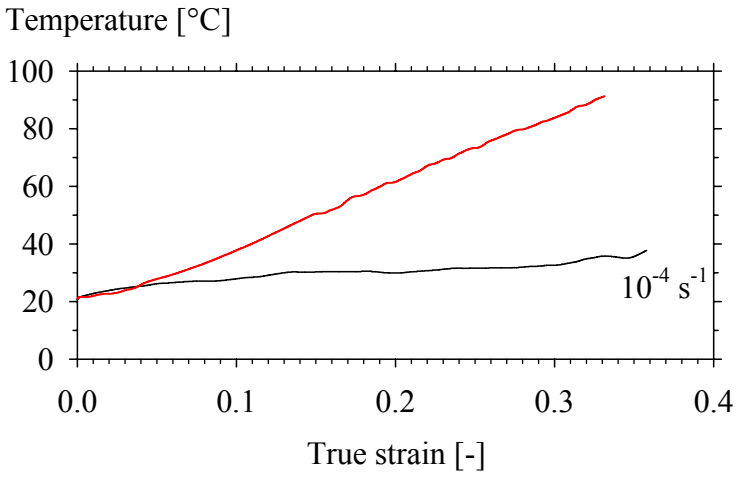

(b)

Figure VI.15 : (a) Tensile true stress vs. true strain curves of steel 301LN using two different strain rates (10^{-4} s^{-1} and 3 10^{-3} s^{-1}) ; (b) Evolution of temperature during straining of samples in (a).

Figure VI.16 shows the evolution of the work-hardening rate during plastic deformation of steel 301LN at two strain rates (10^{-4} s^{-1} or 3 . 10^{-3} s^{-1}). For both samples, $n_{incr.}$ increases during the first part of straining then decreases down to necking. For both samples, the work-hardening rate suddenly rises around $\varepsilon = 0.08$. However, the maximum of $n_{incr.}$ is lower and reached sooner for the higher strain rates.

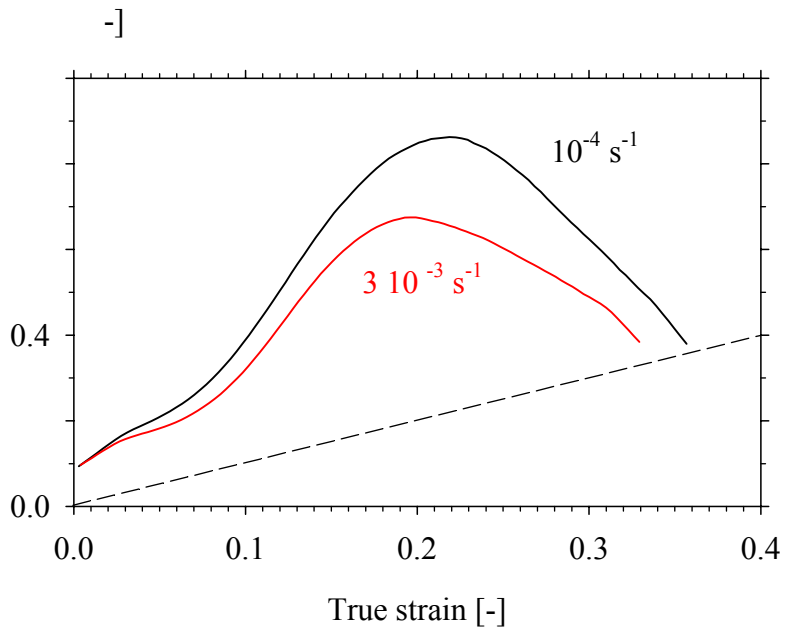

Figure VI.16 : Evolution of $n_{incr.}$ during tensile test of steel 301LN at two different strain rates (10^{-4} s^{-1} and 3 . 10^{-3} s^{-1}). (the dashed line corresponds to the Considere instability criterion).

The evolution of the phase proportions of steel 301LN during tensile straining at different strain rates (10^{-4} s^{-1} and 3 10^{-3} s^{-1}) are presented in Figure VI.17. The evolution of the phase proportions with

straining is similar for both strain rates : the austenite decreases while the α'-martensite increases and the ε-martensite increases, reaches a maximum then decreases. For the smaller strain rate, it can be observed that the transformation of austenite is more complete. No clear difference can be observed between the proportion of ε-martensite in both samples.

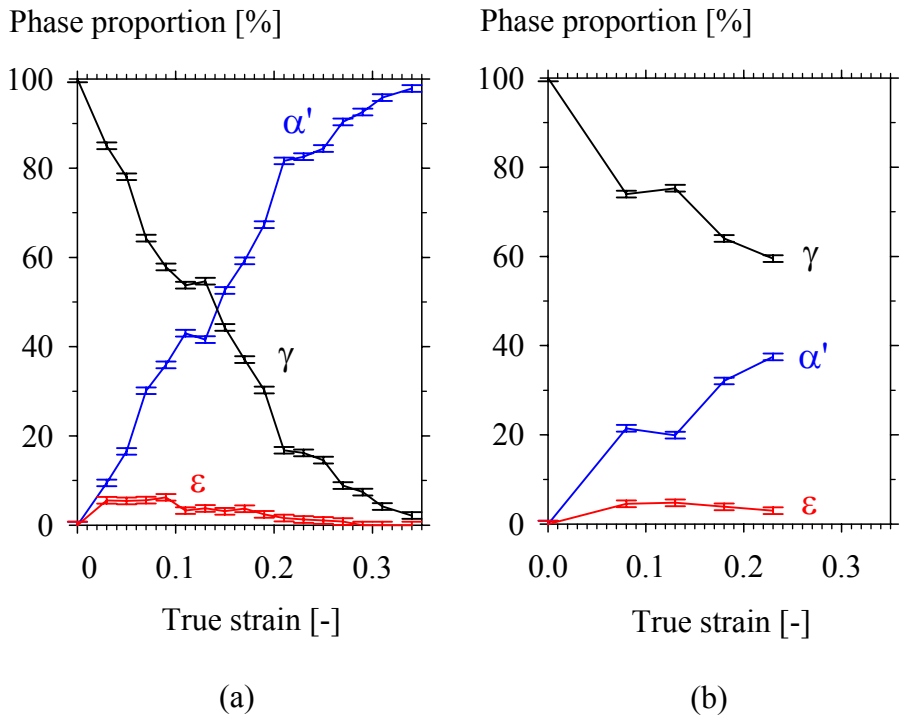

Figure VI.17 : Evolution of the phase proportions during tensile straining at two different strain rates : (a) 10^{-4} and (b) 3 10^{-3}.

VI.3.2 Evolution of phase proportions during cold rolling or rotary swaging in Fe-Ni-Cr stainless steels

Figure VI.18 shows the evolution of the phase proportions present in specimens of steel 301LN deformed by cold rolling (Figure VI.18 (b)) or rotary swaging (Figure VI.18 (c)). For comparison purposes, the evolution of phase proportions in steel 301LN during tensile straining are reminded in Figure VI.18 (a). Figure VI.18 (d) presents the evolution of phase proportions in steel 304 strained by rotary swaging. The transformation rates vary in a large way depending on the deformation technique. The transformation rate decreases from uniaxial tension to cold rolling, and finally to swaging. Furthermore, the maximum amount of ε-martensite also appears earlier in tension than in rolling, while no ε-martensite forms by swaging. Finally, the transformation rate is lower in steel 304 than in steel 301LN.

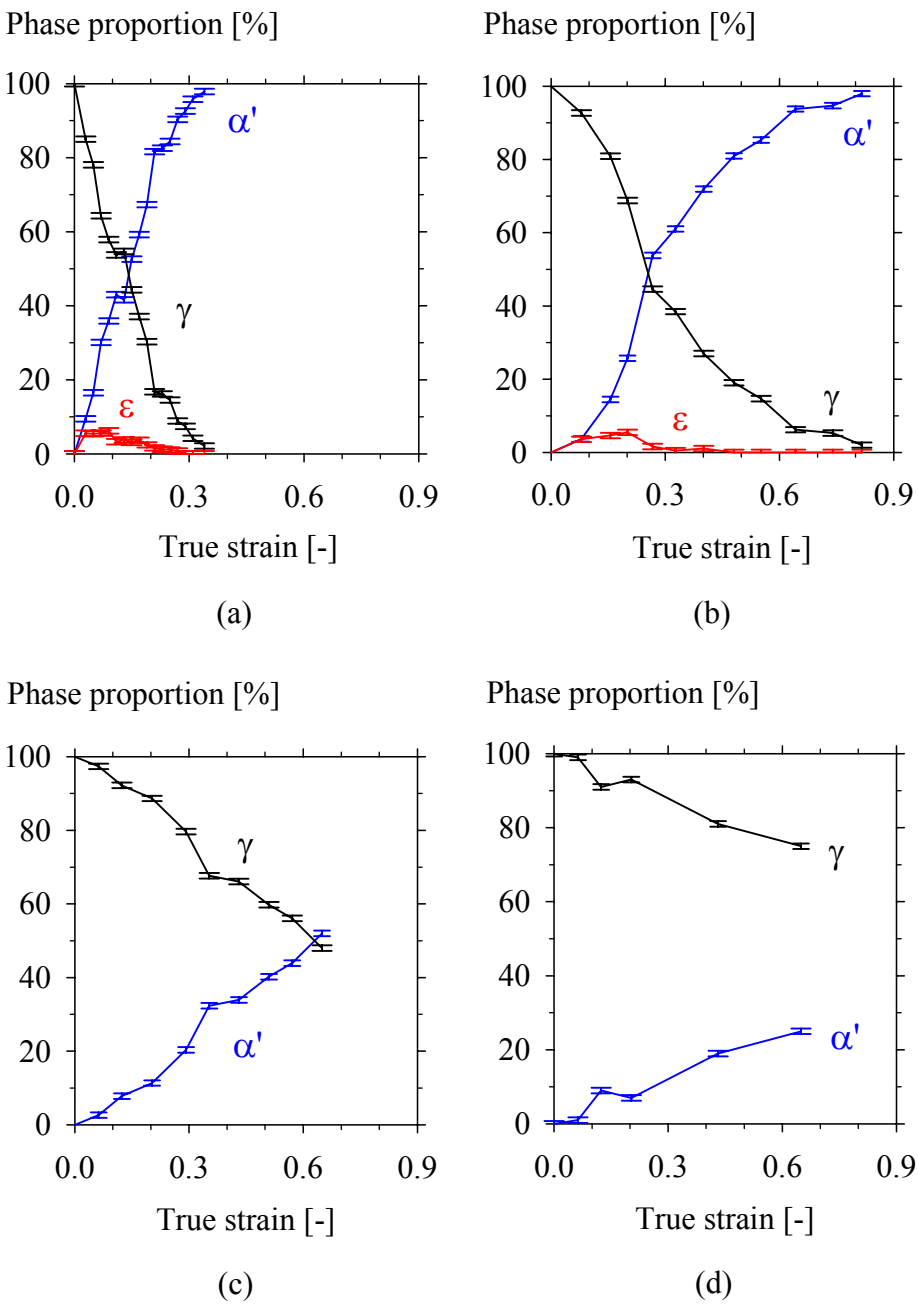

Figure VI.18 : Evolution of the phase proportions in steel 301LN during (a) uniaxial tension ; (b) cold rolling or (c) rotary swaging and (d) in steel 304 during rotary swaging.

VI.4 Discussion

VI.4.1 Role of the different phases in the mechanical properties

VI.4.1.1 Influence of ferrite and austenite on the mechanical properties in Fe-Mn-Si-Al steels

In steels Mn15 and Mn20, the proportions of ferrite and austenite vary as a function of the chemical composition and the annealing temperature. The mechanical properties of these phases are different. Therefore, the phase proportions directly influence the mechanical properties of these alloys. Figure VI.19 presents, for austenite and ferrite in sample Mn15 1000, the lattice strain *vs.* macroscopic true strain during the first stages of tensile deformation. Figure VI.19 (a) shows the estimation of the lattice Young modulus of the phase ($E^{lat.}$) obtained by the linear interpolation of the measurements in the early stages of deformation. It can be seen that the elastic modulus is higher in the austenite (216 GPa) than in the ferrite (170 GPa). Figure VI.19 (b) allows to determine the lattice deformation at yielding. Indeed, when the austenite yields, the stress transfer between the two phases is modified and the ferrite must hold a larger stress, which brings about an abrupt increase in the evolution of the ferrite lattice strain with respect to the macroscopic stress [Jacq06]. The same observations allow to determine the ferrite yield point. Then, from these yield points the lattice strain at phase yielding, $\varepsilon_y^{lat.}$, can be obtained as presented in section II.2.1.3.

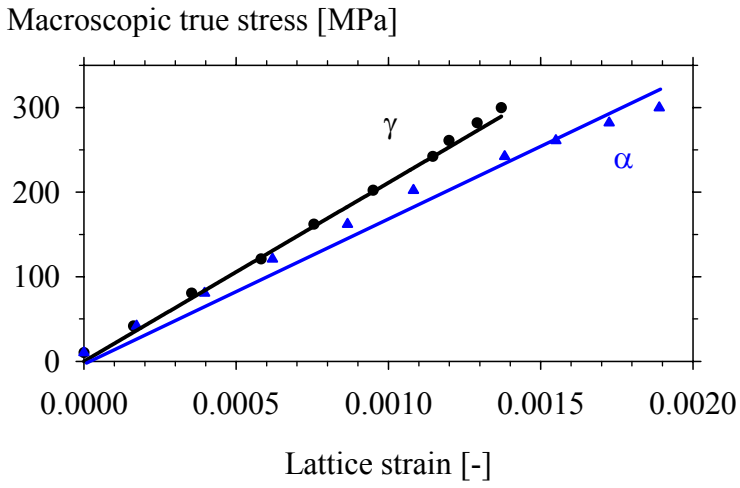

(a)

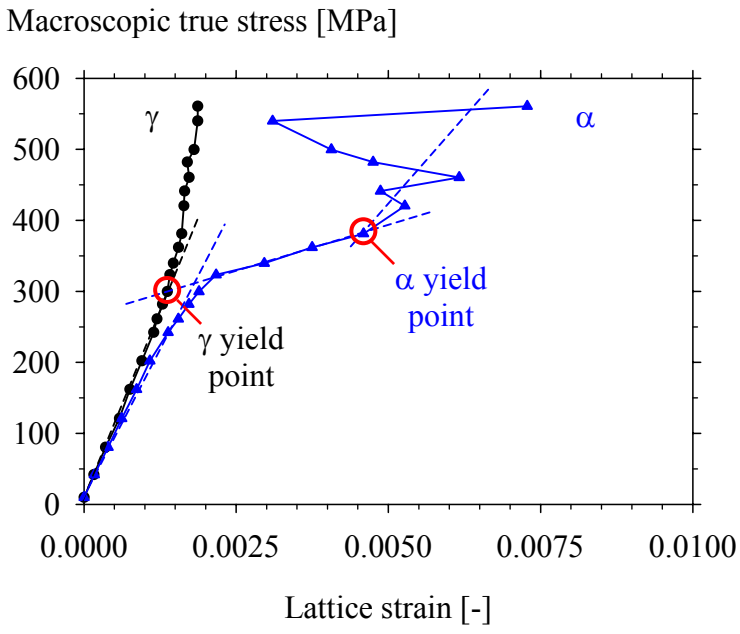

(b)

Figure VI.19 : Lattice strain vs. macroscopic true stress for austenite (γ) and ferrite (α) in sample Mn15 1000 during the first stages of tensile deformation : (a) estimation of the Young modulus of the phases ; (b) determination of the yield point for each phase.

The proportion of ferrite has a strong influence on the mechanical properties due to its larger yield strength compared to austenite. The estimations of lattice strain at phase yielding and phase Young modulus allow an estimation of the yield strength of the different phases $\sigma_y^{lat.}$ in steel Mn15 by :

$$\sigma_y^{lat.} = E^{lat.} \cdot \varepsilon_y^{lat.} \qquad \text{(VI.2)}$$

It can be seen that the austenite presents a lower yield strength than the ferrite (*i.e.* 296 MPa and 779 MPa, respectively). A rule of mixture provides σ_y*(Mn15 1000)*, the yield strength of sample Mn15 1000 :

$$\sigma_y(Mn15\ 1000) = \%\alpha \cdot \sigma_{y,\alpha}^{lat.} + \%\gamma \cdot \sigma_{y,\gamma}^{lat.} \qquad \text{(VI.3)}$$

where *%i* and $\sigma_{y,i}^{lat.}$ stand for the proportion and the yield strength of the phase *i*, respectively. As steel Mn15 1000 contains 45% austenite and 55% ferrite, the yield strength of sample Mn15 1000 is calculated as 562 MPa, which is in good agreement with the macroscopic value measured in tension for sample Mn15 1000.

It is the larger proportion of ferrite combined to the higher yield strength of this phase that dictate the difference of mechanical properties between steels Mn15 and Mn20, especially in the first stages of straining, where little phase transformation has occurred. As a consequence, for a similar grain size, sample Mn15 1000 exhibits a higher yield strength than sample Mn20 900.

VI.4.1.2 Effect of strain-induced phase transformation on the mechanical properties

The strain-induced phase transformation has a key influence on the mechanical properties of both Ni-Cr stainless steels and high Mn alloys. When a phase transformation takes place, the first effect is a softening due to the transformation strain. Indeed, the martensitic transformation brings about a volume increase and a local shear as explained in Chapter I. Moreover, it has been shown in Chapter V that the variants with a transformation strain favourably oriented relatively to the local stress field are formed preferentially. Thereby, the transformation relieves the local stress concentration and the transformation strain induces local plasticity and softens the material. In a second time, a "composite effect" can be invoked, especially if the newly appeared phase is harder than the mother phase. In fact, the replacement of austenite by harder martensite increases the work-hardening after the transformation.

In Fe-Mn alloys, Tomota *et al.* [Tomo86] showed that both ε- and α'-martensite bring about little reinforcing composite effect, due probably to mechanical properties similar to the mother austenite. However, they act as barriers to the progression of dislocations or other phase transformations and thereby brings about reinforcement. In steels Mn15 and Mn20, it appears that only the α'-martensite does provide a strong composite reinforcing effect and even a minor change in its proportion has a great influence on the resistance of the material, whereas the bands of ε-martensite would act mainly as obstacles against plastic deformation. The composite effect is directly related to

the change of curvature of the true stress – true strain curves. Indeed, Figure VI.20 compares the evolution of the work-hardening rate and of the proportions of ε- and α'-martensite (normalised with respect to the initial quantity of austenite) for steels Mn15 900 and Mn20 1000. In steel Mn15 (Figure VI.20 (a)), it can be observed that $n_{incr.}$ increases steeply when the α'-martensite formation rate rises (about $\varepsilon = 0.07$). On the other hand, in steel Mn20 (Figure VI.20 (b)), the α'-martensite forms continuously all along straining and no steep increase of the work-hardening rate can be observed. Finally, in both grades, the proportion of ε-martensite does not seem to influence the work-hardening rate.

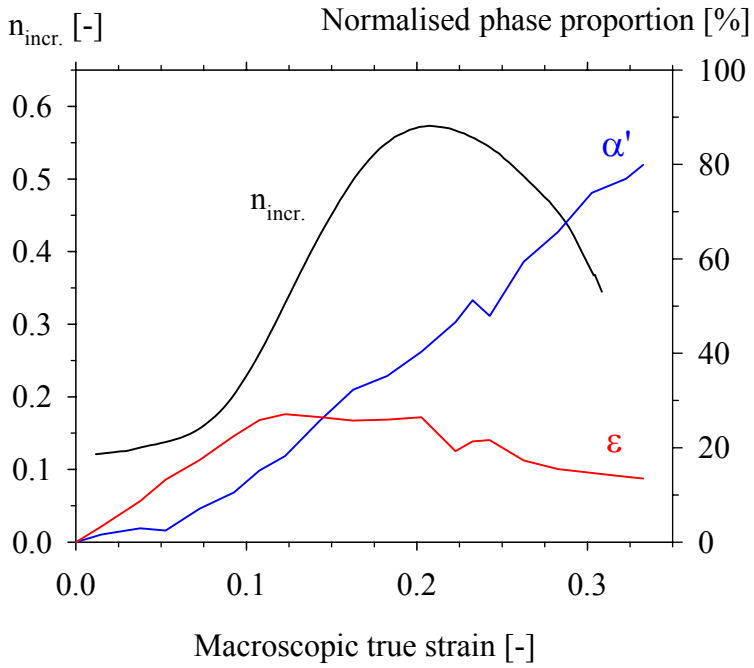

(a)

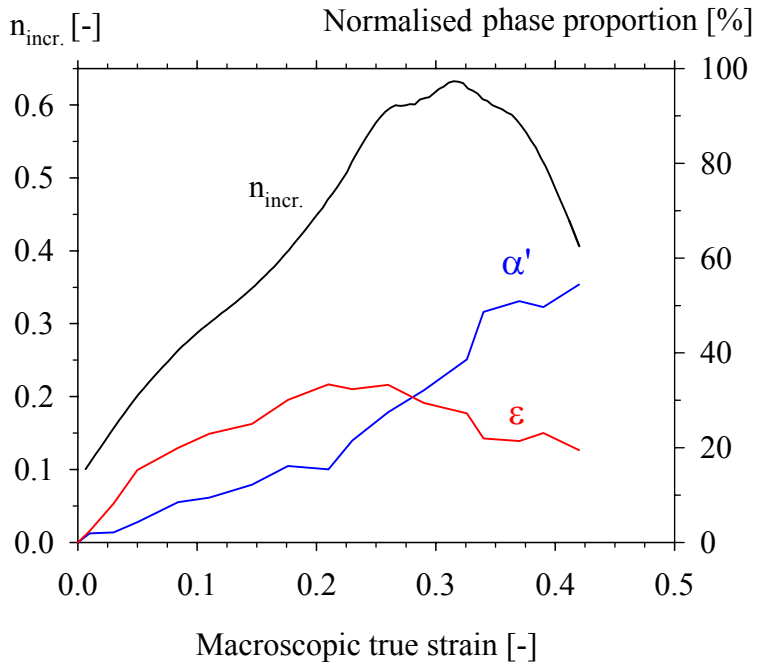

(b)

Figure VI.20 : Evolution of work-hardening rate together with the normalised proportions of α'- and ε-martensite during tensile straining for samples (a) Mn15 900 and (b) Mn20 1000. $\varepsilon^{thr.}$ corresponds to the threshold deformation where the $n_{incr.}$ and the rate of α'-martensite formation start to increase.

The existence of a threshold after which the formation of α'-martensite increases is related to the mechanisms of phase transformations. Indeed, in steels Mn15 and Mn20, the α'-martensite grains nucleate mostly at the intersection of two bands of ε (see chapter V), and grow strictly within the ε bands. Therefore, the formation of α'-martensite is prevented until the relative proportion of

ε-martensite reaches a minimum level (*i.e.* 10 – 12% in steel Mn15). As the formation rate of ε-martensite is higher in steel Mn20, the minimum proportion is reached at a lower strain and no stage is visible in the evolution of the work-hardening rate and in the rate of α' formation.

In steel 301LN, the influence of the phase transformations on the mechanical properties can be deduced from the effect of the change of strain rate. Indeed, the variation of strain rate in the studied range has almost no direct influence on the mechanical properties, as it is shown by the slight influence on the yield strength (Figure VI.15). However, the transformation rate decreases when the strain rate increases. Indeed, a higher strain rate prevents the heat to be dissipated during straining and brings the conditions closer to adiabatic conditions. In the samples 301LN, it induces a progressive heating during straining and the difference of temperature due to the strain rate reaches its maximum of about 60°C at necking of the first sample. The impact of a progressive rise of 60°C on the mechanical properties of the austenite is negligible but it has a large effect on the transformation rate. Talonen *et al.* [Talo05] proved that the same observations can be made for much higher strain rates (up to 200 s^{-1}). As far as the mechanical properties are concerned, it may be seen on Figure VI.15 and VI.16 that the tensile and the work-hardening rate curves are very similar for both strain rates up to $\varepsilon = 0.05$. Then, the temperature increase in the sample tested at a high strain rate starts to be noticeable and the gap between the curves increases as the reinforcement by phase transformation is reduced. However, the $\gamma \rightarrow \varepsilon$ transformation

seems much less affected by the temperature rise so that it may be concluded that the work-hardening brought about by the phase transformation is essentially due to the formation of α'-martensite. Lebedev and Kosarchuk [Lebe00] reached the same conclusions by comparing two different austenitic stainless steel grades at different temperatures. Indeed, they observed that for two grades having similar tensile curves at room temperature, the grade which forms more α'- and less ε-martensite also presents a higher work-hardening rate.

VI.4.2 Influence of the chemical composition on the mechanical properties and on the strain-induced transformations

The effect of the difference in Mn content on the mechanical properties of steels Mn15 and Mn20 is twofold : first, it induces different initial phase proportions, then it affects the phase transformations. As it has been shown in Chapter III, a higher Mn content decreases the proportion of ferrite. As the yield strength of ferrite is higher, the level of stress is expected to be higher in steel Mn15 than in steel Mn20 for the same strain. The higher solution strengthening effect due to the presence of Mn [Caba04] is secondary compared to the variation of initial phase proportions and can be neglected.

Moreover, the phase transformations are also affected by the higher Mn content. The comparison between the evolution of phase proportions with deformation for samples Mn15 1000 (Figure VI.8)

and Mn20 900 (Figure VI.9) illustrates the influence of the manganese content on the phase transformations. Indeed, the concentration of Mn is the only varying parameter as the austenite in these two samples have similar grain size (11µm and 12µm, respectively), silicon content (2.8 wt.% and 2.88 wt.%, respectively) and aluminium content (2.69 wt.% and 2.88 wt.%, respectively). Figure VI.21 shows the evolution as a function of the macroscopic true strain of the phase proportions normalised with respect to the initial quantity of austenite in samples Mn15 1000 and Mn20 900. It shows that the transformation rate of austenite and the rate of formation of α'-martensite are proportionally larger in sample Mn15 1000 than in sample Mn20 900.

Due to the difference in the phase proportions, the macroscopic true stress is higher in steel Mn15 than in steel Mn20 for the same strain level. Therefore, the average level of stress within the austenite is expected to be higher in steel Mn15 than in steel Mn20, which favours the phase transformations. Moreover, the Mn content also influences directly the phase transformations, as it modifies the SFE and the austenite stability. Indeed, according to the thermodynamic model presented in Chapter III, the SFE of grades Mn15 and Mn20 are about 9 mJ/m² and 15 mJ/m² at room temperature, respectively. Moreover, a higher Mn content stabilizes the austenite (Chapter I). Therefore, a higher Mn content also reduces the phase transformations in steel Mn20 with respect to steel Mn15.

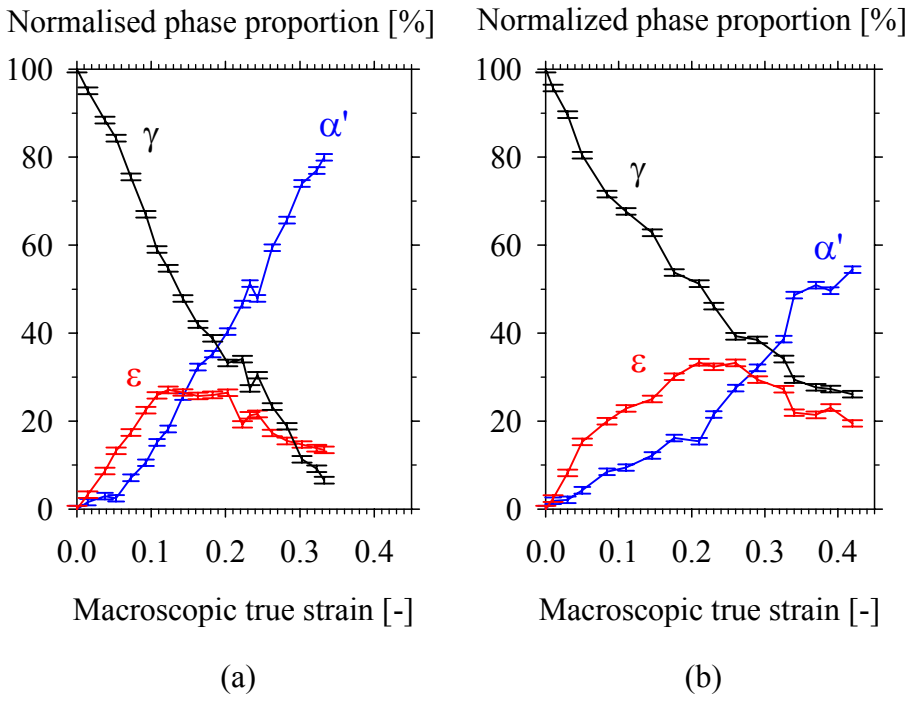

Figure VI.21 : Evolution during tensile straining of normalised phase proportions for samples (a) Mn15 1000 and (b) Mn20 900.

In stainless steels, the chemical composition and the temperature have a first range order influence on the phase transformations. Figure VI.22 presents the evolution of the α'-martensite proportion during tensile straining in steel 304 at various temperatures (from [Shin01]) as well as in the present steel 301LN. It can be observed that when the temperature increases, the transformation rate decreases, and that the transformation rate at room temperature is smaller in steel 304. The later observation can also be made by comparing the formation of α'-martensite during rotary swaging in steels 301LN (Figure VI.18 (b)) and 304 (Figure VI.18 (d)).

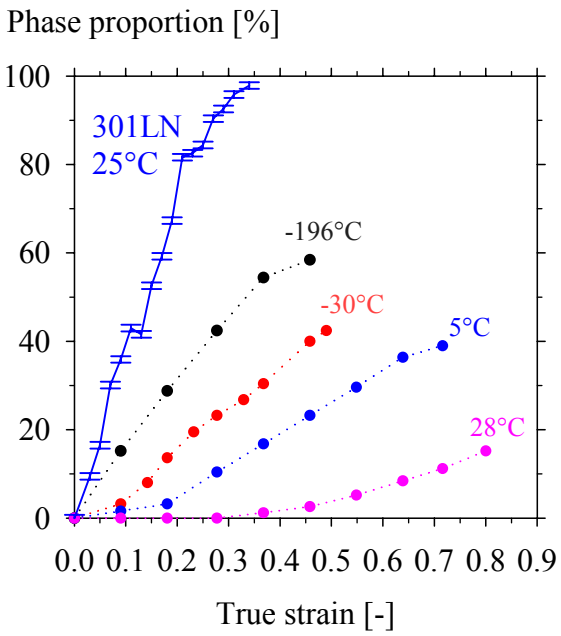

Figure VI.22 : Evolution of α'-martensite proportion during tensile straining in steel 304 at different temperatures (from [Shin01]) and in steel 301LN.

The stacking fault energy of stainless steels can be estimated by the linear relationship I.3 presented in section I.2.2.1 and based on the alloying contents of stainless steels :

$$\text{SFE (in mJ/m}^2\text{)} = -53 + 0.7\,(\%\,\text{Cr}) + 6.2\,(\%\,\text{Ni}) + 3.2\,(\%\,\text{Mn}) + 9.3\,(\%\,\text{Mo}) \qquad \text{(VI.4)}$$

The SFE of grades 301LN and 304 are estimated to 5.8 mJ/mm² and 23.2 mJ/mm², respectively. Indeed, the Ni and Cr content of steel 304 are higher than for steel 301LN. Moreover, as the Ni has a strong gamma-stabilising effect, the combination of an increase in SFE and

austenite stability explains the decrease of transformation rate in steel 304 compared to steel 301LN. However, the mechanisms of phase transformations in grade 304 are identical to the ones observed in this work for grade 301LN [Spenc04a, Gey05]. As a consequence, the higher transformation rate leads to a quick increase of the work-hardening rate and to higher stresses at maximum loads.

VI.4.3 Influence of the temperature on the mechanical properties and on the strain-induced transformations in Fe-Ni-Cr stainless steels

Globally, an augmentation of temperature causes a SFE increase and stabilises the austenite against phase transformations. The approximation of Dai *et al.* [Dai03] presented in section I.2.2.2 evaluates the influence of the temperature on the SFE as :

$$SFE = SFE_1 + 0.07\,(T - T_1) \qquad \text{(VI.5)}$$

with SFE_1 being the SFE at room temperature T_1. Applied on 301LN steel, it predicts that for a SFE of 5.8 mJ/mm² at room temperature, the SFE at 72°C (temperature reached at the end of the tensile test at a strain rate of $3 \cdot 10^{-3}$ s^{-1}) would be about 9.4 mJ/mm². Based on the estimations for the selection of the deformation mode presented in section I.2.3.4, no change of transformation mechanism should be brought about by such a SFE increase. Moreover, the austenite is more stable at higher temperatures. The temperature rise would thus essentially affect the transformation rate due to its effect on the SFE

and on the relative stability of the phases. For example, rolling tests performed on 301LN steel at just 200°C showed that no phase transformation occurred at this temperature (see Chapter IV). These conclusions are in good agreement with what is observed in steel 304 [Shin01].

VI.4.4 Influence of the austenite grain size on the mechanical properties and on the strain-induced transformations

In all metals, a larger grain size decreases the yield strength and the resistance and increases the ductility. Indeed, larger grains means lower density of grain boundaries, which behave like obstacles to the dislocation movement. The effect on the strength can be expressed thanks to the Hall-Petch relationship [Kash95] :

$$\sigma(\varepsilon) = \sigma_0(\varepsilon) + k_y(\varepsilon) \cdot d^{-0.5} \qquad \text{(VI.6)}$$

where $\sigma(\varepsilon)$ is the flow stress corresponding to the grain size d, and $\sigma_0(\varepsilon)$ and $k_y(\varepsilon)$ are constant at given strain (ε) and temperature. It can be seen that a larger grain size reduces the flow stress.

Moreover, increasing the austenite grain size favours the phase transformation. The origin of this effect lies in the decrease of the stacking fault energy (SFE) observed in larger austenite grains as presented in section I.2.2.4. Moreover, the martensitic transformation can be hindered by the density of defects in the mother austenite, such

as grain boundaries or previously formed variants of martensite [Lani05].

In Fe-Mn-Si-Al steels, the variation of grain size in the studied range has only a minor influence on the phase transformations. Indeed, the strongest variation of austenite grain size is found between samples Mn20 900 and Mn20 1000 (12µm and 23µm, respectively). As the proportion and composition of the austenite are similar in both samples, the difference of transformation rates and mechanical properties may be essentially attributed to this variation of grain size, although the influence on the phase transformations is limited.

The effect of the grain size on the yield strength, the resistance and the ductility is very clear in stainless steels, as it is shown on Figure VI.12. As it has been shown, there is a direct relationship between the rate of formation of α'-martensite and the evolution of the work-hardening rate in stainless steels. Therefore, the stage in the evolution of the work-hardening rate in steel 301LN with grain size of 1.2µm (see Figure VI.13) can be related to the evolution of phase proportions presented in Figure VI.14. Indeed, for the small grained sample, a stage is also visible in the formation rate of α'-martensite for similar levels of strain.

In steel 301LN, Figure VI.14 showed that a lower austenite grain size reduces the austenite transformation rate. This could be due to a rise of the SFE and austenite stability induced by the smaller grain size. However, the small-grained sample exhibits a higher proportion

of α'-martensite in the first part of the straining. This could be explained by the higher yield stress due to the small grains. Indeed, the high yield stress may induce larger martensitic transformation in the sample in a first stage. Then, further transformation may have been hindered due to the effect of high defects density until the energy barrier could be overcome at larger strain levels.

VI.4.5 Influence of the stress state on the phase transformations in Fe-Ni-Cr stainless steels

The influence of the deformation mode on the rate of phase transformation depends mainly on the sample heating and on the loading path. Uniaxial tension and cold rolling were carried out at low strain rates, so that the samples temperature was more or less constant all along straining. These two modes of deformation thus differ only by the loading path, which can be characterised by the macroscopic stress triaxiality ratio (*TR*) and the Lode parameter (*LP*). These factors are reminded for the different deformation modes in Table VI.3.

Deformation mode	*TR*	*LP*
Uniaxial tension	$\frac{1}{3}$	*-1*
Cold rolling	$-\frac{\sqrt{3}}{3}$	*3*
Rotary swaging	$-\frac{2}{3}$	*1*

Table VI.3 : Estimation of the stress triaxiality ratios and Lode parameters for uniaxial tension, cold rolling and rotary swaging.

The influence of *TR* on the transformation rate is related to the relationships between the transformation strain and the sign of the applied stress. Indeed, the formation of α'-martensite brings about a volume expansion which is favoured under tensile stress [Pate53, Stri92]. On the other hand, as the formation of ε-martensite is accompanied by a volume reduction, the inverse influence can be observed and the formation of ε phase is increased under compressive stress [Lebe00].

However, previous works [Lebe00, Furn03, Lani05] have shown that the influence of the stress triaxiality ratio is not monotonous. For example, the change from uniaxial tension to biaxial tension corresponds to an increase of the stress triaxiality ratio even though the rate of α' formation decreases [Lebe00]. This can be explained by the effect of the Lode parameter (*LP*), describing the stress deviator, which increases in this case. The increase of *LP* is directly related to the shear component of the stress in biaxial tension. The retarding effect on the martensitic transformation is explained by the formation of a more complex stressed austenite structure with an increased density of structural defects. This increased defect density could also hinder the reorganisation from one lattice to the other [Lani05]. Rotary swaging exhibits the lowest *TR* but an intermediate *LP* compared to the two other methods. The transformation level would be expected to be lower than in tension but higher than in rolling. However, the rapid heating in the case of the swaging changes the austenite stability so that direct comparison is not straightforward. Finally, it is worth noting that the redundant work and surface shear

phenomena observed during the rotary swaging bring about more shear and plasticity within the material, favouring the phase transformation.

The use of a simple model to estimate the level of phase transformation can be used to reduce the amount of mechanical tests. Spencer *et al.* [Spenc04b] developed a simple geometric model which describes the formation of strain-induced α'-martensite in stainless steel and takes the transformation strain into consideration. This model is based on three major assumptions, based on TEM observations and mechanical tests :

1. There is a critical strain (defined as ε^*) required to generate bands of ε (HCP) from stacking faults.
2. The α'-martensite nucleates only at the intersection of two bands of ε-martensite.
3. The α'-martensite will not grow beyond the intersection volume of two bands.

The second assumption is quite reasonable at the light of experimental results. The third assumption is a simplification, based on the observation that the major part of α'-martensite does form in the intersection volume. This simplification leads to an overestimation of the amount of ε-martensite that forms. However, it is the amount of α'-martensite that is described by the model. It is assumed that all three phases undergo the same plastic strain. The rate of formation of ε bands per unit strain is also assumed constant, and the $\gamma \rightarrow \alpha'$ transformation strain (ε_T) is taken to be 3%.

The model is expressed as :

$$\varepsilon = \varepsilon_T \phi^2 - \varepsilon^* ln(1 - \phi) \qquad \text{(VI.7)}$$

where ϕ represents the volume fraction of both ε- and α'-martensites and ϕ^2 stands for the volume fraction of α'-martensite alone. The model was found to provide a good approximation of the evolution of phase proportions in the case of stainless steel 304 strained at 77K, as it is shown on Figure VI.23.

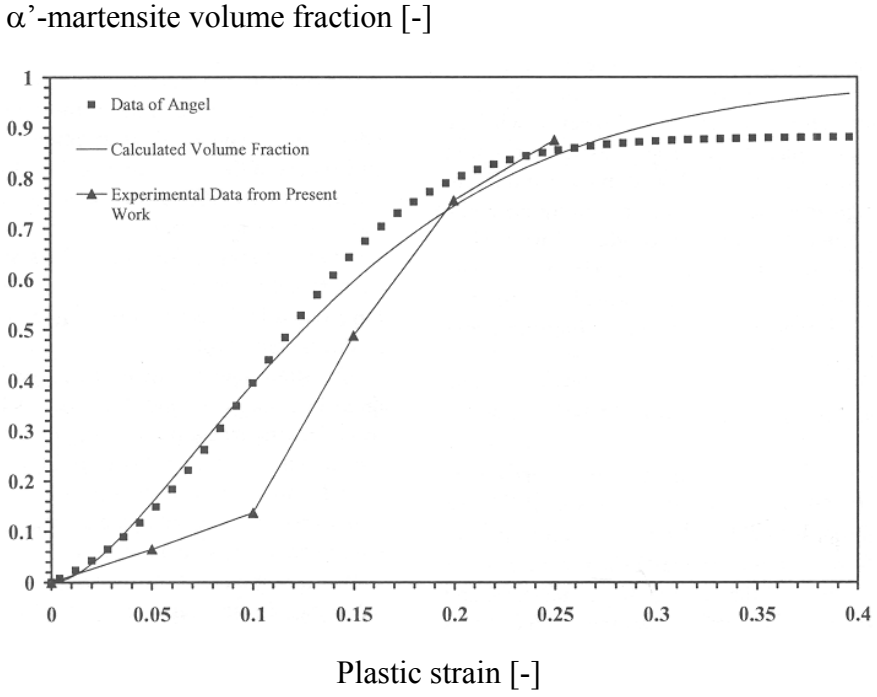

Figure VI.23 : Plot of computed α'-martensite volume fraction as a function of plastic strain at 77K, superimposed upon experimental data of Spencer and of Angel (from [Spen04b]).

As shown in Figure VI.24, this model fits quite well with the volume fractions of α'-martensite from the present results. The values used for the critical strain for transformation (ε^*) are 0.085 for tension, 0.2 for rolling and 0.5 for swaging, respectively. The increase of ε^* corresponds to the effect of the stress state as described in the previous section.

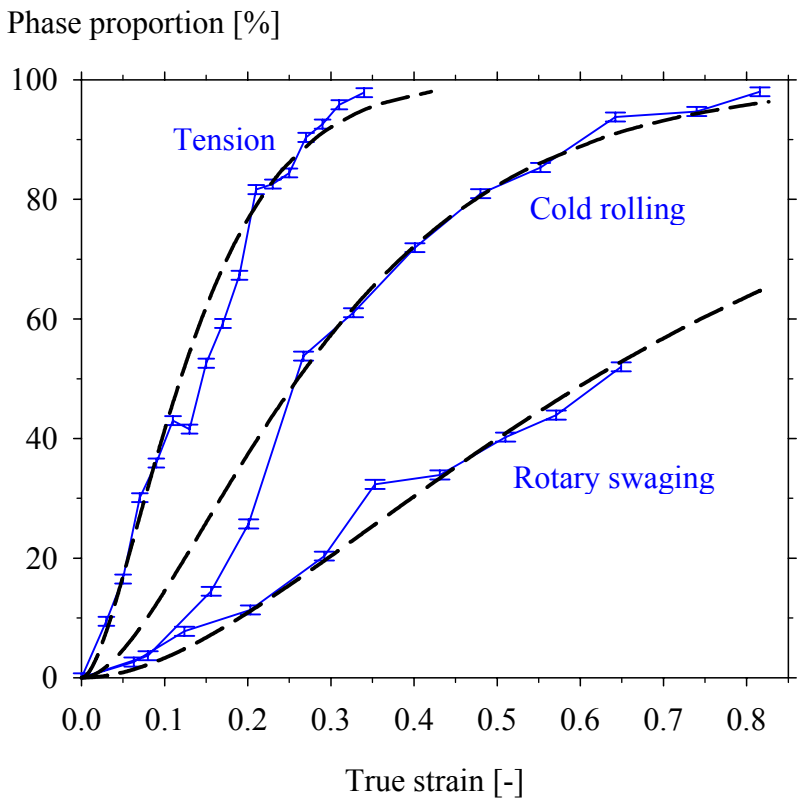

Figure VI.24 : Comparison of the α'-martensite volume fraction as a function of plastic strain measured experimentally and computed by the model of Spencer et. al [Spen04b] for tension, cold rolling and rotary swaging.

VI.5 Conclusion

This Chapter studies the role of the different phases and of the phase transformations on the mechanical properties in stainless steels 301LN and 304, as well as in Fe-Mn-Si-Al alloys Mn15 and Mn20. In particular, the influence of four different parameters was investigated : chemical composition, strain rate and temperature, austenitic grain size and stress state.

In steels Mn15 and Mn20, the ferrite presents a higher yield strength than the austenite. Moreover, the lower Mn content brings about a higher proportion of ferrite in steel Mn15. As a consequence, steel Mn15 displays a higher yield strength than steel Mn20.

In both high Mn alloys and stainless steels, the work-hardening rate is directly related to the formation of α'-martensite. However, the influence of ε-martensite on the work-hardening rate seems to be limited. The mechanisms of formation of α'-martensite are different in stainless steels and in high Mn grades :

- Chapter V showed that in steels Mn15 and Mn20, the α'-martensite nucleates mostly at the intersection of two ε bands and grows strictly within the ε bands. As a consequence, the formation of α'-martensite is reduced up to the point where about 10-12% of the austenite has transformed into ε-martensite. Then, the nucleation of α' grains is increased and the formation rate increases

abruptly. The proportion of ε phase increases, reaches a maximum then decreases during straining.

- During straining of stainless steels, the proportion of ε phase increases, reaches a maximum then decreases until it reaches zero. Indeed, the α' grains nucleate on ε bands but grow also within the austenite (see Chapter V). Therefore, the transformation into α'-martensite may continue even in the absence of ε phase. After rotary swaging, no ε-martensite is observed.

In the high Mn grades, it has been shown in Chapter III that a higher Mn content stabilises the austenite and rises the austenite stacking fault energy (SFE), which reduces the phase transformations. Moreover, the modification of the phase proportions brought about by the increase of Mn content also affects the stress level in the austenite. This effect plays a capital role in the reduction of phase transformations. In the stainless steels, an increase of the Ni content stabilises the austenite and an increase of the Ni and Cr contents rises the SFE. The combination of these effects tends to reduce the phase transformation rate and intensity in stainless steels with higher Ni- and Cr-proportions. The chemical composition exhibits the strongest influence on the mechanical properties both in stainless steels and in high Mn alloys.

In stainless steels, a change of strain rate between 10^{-4} s^{-1} and $3 \cdot 10^{-3}$ s^{-1} has no direct influence on the mechanical properties but increases the sample temperature. A temperature rise, either due to a

higher testing temperature or strain rate, increases the SFE and stabilises the austenite, bringing about a decrease in the intensity and in the rate of phase transformations. Moreover, a smaller austenitic grain size also reduces the phase transformation. Finally, a higher stress triaxiality enhances the phase transformation as the applied stress tends to have a more favourable influence on the transformation strain. A lower Lode parameter has the same effect, as it corresponds to a more favourable shear component in the applied stress.

References :

[Caba04] N. Cabañas Poy, **Compositional effects on Structure-Property relationships in Mn-based austenitic ferrous alloys**, PhD Thesis, Ghent University, 2004.

[Cote04] S. M. Cotes, A. Fernández Guillermet and M. Sade, *Metal. and Mater. Trans. A*, 2004, Vol. 35A, p. 83.

[Char81] J. Charles and A. Berghezan, *Cryogenics*, 1981, p. 278.

[Chen93] F. C. Chen, C. P. Chou, P. Li and S. L. Chu, *Mater. Sci. Eng. A*, Vol. 160, 1993, p. 261.

[Dai03] Q. X. Dai, X. N. Cheng, X.M. Luo and Y. T. Zhao, *Materials Characterization*, Vol. 49, 2003, p. 367.

[Dai04] Q. X. Dai, X. N. Cheng, Y. T. Zhao, X.M. Luo and Z. Z. Yuan, *Materials Characterization*, Vol. 52, 2004, p. 349.

[From03] G. Frommeyer, U. Brüx and P. Neumann, *ISIJ International*, 2003, Vol. 43, p. 438.

[Furu89] T. Furukawa, *Materials Science and Technology*, 1989, Vol. 5, p. 465.

[Furn03] Q. Furnemont, **The micromechanics of TRIP-assisted multiphase steels**, PhD Thesis, UCL, 2003.

[Gey05] N. Gey, B. Petit and M. Humbert, *Metal. and Mater. Trans. A*, 2005, Vol. 36A, p. 1957.

[Good70] D. Goodchild, W. T. Roberts and D. V. Wilson, *Acta Metal.*, 1970, Vol. 18, p. 1137.

[Gräs98] O. Grässel and G. Frommeyer, *Materials Science & Technology*, 1998, Vol. 14, p. 1213.

[Jacq06] P.J. Jacques, Q. Furnemont, S. Godet, T. Pardoen, K. T. Colon and F. Delannay, *Philosophical Magazine*, 2006, Vol. 86, No. 16, p. 353.

[Jun98] J. H. Jun and C. S. Choi, *Mater. Sci. Eng. A*, 1998, Vol. 257, p. 353.

[Kash95] B.P. Kashyap and K. Tangri, *Acta Metall. Mater.*, Vol 43, No 11, 1995, p. 3971.

[Laco90] **Les aciers inoxydables**, 1990, edited by P. Lacombe, B. Baroux and G. Beranger for « Les éditions de Physique ».

[Lani05] F. Lani, **Micro-mechanical modelling of dual-phase elasto-plastic materials**, PhD Thesis, UCL, 2005.

[Lebe00] A. A. Lebedev and V. V. Kusarchuk, *International Journal of Plasticity*, 2000, Vol. 16, p. 749.

[Lee00] Y. K. Lee and C. S. Choi, *Metal. and Mater. Trans. A*, 2000, Vol. 31A, p. 355.

[Oh95] B. W. Oh, S. J. Cho, Y. G. Kim, Y. P. Kim, W. S. Kim and S. H. Hong, *Mater. Sci. Eng. A*, 1995, Vol. 197, p. 147.

[Patel53] J. R. Patel and M. Cohen, *Acta Metall.*, 1953, Vol 1, p 531.

[Shin01] H. C. Shin, T. K. Ha and Y. W. Chang, *Scripta Mat.*, 2001, Vol. 45, p. 823.

[Spen04a] K. Spencer, **The work hardening of austenitic stainless steel, applied to the fabrication of high-strength conductors**, PhD Thesis, Mc Master University, 2004.

[Spen04b] K. Spencer, J. D. Embury, K. T. Conlon, M. Véron and Y. Bréchet, *Mater. Sci. Eng. A*, 2004, A387-389, p. 873.

[Stri92] R. G. Stringfellow, D. M. Parks and G. B. Olson, *Acta Metall. Mater.*, 1992, Vol. 40, No. 7, p. 1703.

[Talo04] J. Talonen and H. Hänninen, *Metal. and Mater. Trans. A*, 2000, Vol. 35A, p. 2401.

[Talo05] J. Talonen, P. Nenonen, G. Pape and H. Hänninen, *Metal. and Mater. Trans. A*, 2005, Vol. 36A, p. 421.

[Tomo86] Y. Tomota, M. Strum and J. W. Morris Jr., *Met. Trans. A*, 1986, Vol. 17A, p. 537.

[Tomo91] Y. Tomota, *Institute of Japan*, 1991, Vol. 77 No. 3, p. 315.

[Verc04] S. Vercammen, Processing and tensile behaviour of TWIP steels : microstructural and textural analysis, PhD Thesis, KUL, 2004.